Tian, Y. & Senetakis, K. *Géotechnique* [https://doi.org/10.1680/jgeot.20.P.208]

Influence of creep on the small-strain stiffness of sand–rubber mixtures

YU TIAN* and KOSTAS SENETAKIS†

A series of bender element tests was carried out to investigate the variation of small-strain stiffness (G_{max}) of sand–granulated rubber mixtures under long-term loading. Comparisons were made using two different host sands: a non-crushable material called Sydney sand and a crushable material composed of completely decomposed volcanic rock (CDV). The test results suggested that, at the selected stress states in the study (mean effective confining stress ranged from 250 to 333 kPa), the influence of creep on the stiffness of the pure sand specimens was more pronounced for CDV compared with Sydney sand and the presence of rubber amplified creep effects on both types of mixtures. The influence of creep on G_{max} was therefore associated with two major mechanisms: the increased compressibility of specimens predominantly because of grain crushing (contribution of sand fraction), and the increased compressibility because of the presence of soft rubber grains (contribution of the rubber fraction). The significant influence of grain breakage on the relationship between stiffness and creep was confirmed by post-test examination of the grain-size distribution curves of pure CDV samples. For rubber–CDV mixtures, the inclusion of soft and viscoelastic rubber grains prevented breakage, in this way reducing the creep mechanism due to grain crushing, but increased the overall influence of creep on stiffness. These conclusions were drawn based on 20% of rubber by mixture weight, and very similar behaviour was observed for 10% rubber. It was therefore understood that the aggravation of creep induced by the increased deformations due to the presence of rubber, for the given contents of rubber included in the study, was more dominant compared with the adverse influence of rubber on samples' creep by preventing sand grain breakage.

KEYWORDS: creep; geosynthetics; residual soils; stiffness

INTRODUCTION

Mixing rubber in a granulated or shredded form with geomaterials has received great attention in geotechnical engineering research and practice in recent decades. Applications of sand–rubber mixtures and also pure granulated rubber include their use as lightweight backfill behind retaining walls (Humphrey & Sandford, 1993; Bernal *et al*., 1997) and reinforcing geosynthetic of weak subgrades (Edinçliler & Cagatay, 2013). Laboratory research works have also suggested that, within an optimum range of contents of rubber, soil–rubber mixtures may have improved strength so that the rubber grains may provide a reinforcing mechanism (Foose *et al*., 1996; Edil, 2002; Zornberg *et al*., 2004; Edinçliler & Ayhan, 2010). The optimum contents of rubber may vary, based on different factors, but the state-of-the-art literature would suggest that contents of rubber by mixture weight within a range of 15–25% are where the behaviour is sand-dominant or within the transition from sand-dominant to rubber-dominant (ASTM, 1998; Zornberg *et al*., 2004; Kim & Santamarina, 2008; Edil, 2012; Senetakis *et al*., 2012; Lopera Perez *et al*., 2017a; Li *et al*., 2019a). A higher damping ratio of the mixtures, compared with that of pure soils, also extends their applications to seismic hazard mitigation projects (e.g. Tsang, 2008; Senetakis *et al*., 2012; Senetakis & Anastasiadis, 2015; Tsiavos *et al*., 2019). However, the literature suggests that the properties of geosynthetics may change significantly because of creep (i.e. changing properties with an elapsed time); this has been attributed to the viscoelastic nature of geosynthetics resulting in time-dependent behaviour (Wu & Helwany, 1996; Fannin, 2001; Kongkitkul *et al*., 2007; Allen & Bathurst, 2002; Liu, 2012; Nuntapanich *et al*., 2018).

With respect to the influence of creep on the behaviour of soils, it has been reported in the literature that creep results in increasing shaft resistance in driven piles (Chow *et al*., 1998), increasing cone penetration test (CPT) resistance (Mesri *et al*., 1990), reduced dilation angle (Chen & Zhang, 2016) and increasing shear strength (Daramola, 1980; Howie *et al*., 2002). Published works have also studied the changes of the dynamic properties of soils because of creep, with two major observations to be reported as (*a*) increasing small-strain stiffness, G_{max} (Anderson & Stokoe, 1978; Jovičić & Coop, 1997; Gao *et al*., 2012; Wang & Gao, 2013) and (*b*) decreasing damping ratio (Wang & Tsui, 2009). For pure sand, crushing and re-arrangement of grains, which lead to fabric changes, have been reported as important contributing mechanisms associated with creep (Kuhn & Mitchell, 1993; Bowman & Soga, 2003; McDowell, 2003; McDowell & Khan, 2003).

With regard to the creep of sand–rubber mixtures, Ngo & Valdes (2007) have verified with oedometer tests that the strains induced by creep increase with increasing rubber fraction, while Anastasiadis *et al*. (2012a) showed that the influence of creep on the stiffness of sand–rubber mixtures becomes more significant when the rubber content increases. However, that study was limited in that it only investigated the stiffness component, G_{vh} (i.e. propagating waves along the axis of the specimen, while grain polarisation takes places

Manuscript received 21 June 2020; revised manuscript accepted 11 February 2021.
Discussion on this paper is welcomed by the editor.
* Department of Architecture and Civil Engineering, City University of Hong Kong, Kowloon, Hong Kong, China.
† Department of Architecture and Civil Engineering, City University of Hong Kong, Kowloon, Hong Kong, China (Orcid:0000-0003-0190-4768).

radially), of specimens composed of non-crushable sand subjected to isotropic stress paths. In engineering practice, stiffness in different directions (i.e. G_{vh}, G_{hh}, G_{hv}) may vary differently with time. In addition, the host sand may have highly crushable grains (e.g. materials composed of decomposed igneous rocks, the grains of which may crush even at very small confining pressures compared with what occurs in quartz-type sands), and the stress conditions may also be complex. Consequently, extending the study to investigate the relationship between stiffness in different directions against the duration time of constant confinement considering different types of host sands and loading paths is of particular importance to understand and model the long-term performance of geosynthetic systems. In this study, the aim is to provide some insights and quantify the influence of creep on the stiffness of sand–rubber mixtures, exploring the relative roles of sand type (e.g. contribution of grain crushability) and rubber inclusion on the creep behaviour of these composites.

MATERIALS AND TESTING PROGRAMME

Testing materials

Sydney sand and a completely decomposed volcanic rock (denoted CDV) were selected as the host soils and they were mixed with granulated rubber (denoted GR). Sydney sand is a quartz sand and its particles are expected to be non-crushable under the stress states in the current study (maximum applied mean effective confining stress and deviatoric stress: $p' = 333$ kPa, $q = 250$ kPa). CDV is a material with potential applications particularly in tropical and sub-tropical regions such as Hong Kong; this material has very crushable grains and it is expected to be more susceptible to soil creep compared with Sydney sand. Representative scanning electron microscopy (SEM) images of the materials are shown in Fig. 1. Compositional analysis and micromechanical-based characterisation of typical quartz grains and decomposed volcanic grains that are similar to the studied materials have been presented in recently published works (e.g. Sandeep & Senetakis, 2017; Sandeep *et al.*, 2018). The granulated rubber is composed of waste automobile tyres, which had been subjected to a shredding process; the material was purchased from a local commercial supplier. The recycled tyre shreds tested in the study are classified as granulated rubber based on ASTM D6270-98 (1998). The grain size characteristics (mean grain size and coefficient of uniformity) and the specific gravity of solids of the two host sands and the granulated rubber are summarised in Table 1. The grading curves of the materials are illustrated in Fig. 2. Some slight differences of the grading curves of the two sands are observed, which are expected to have a very minor influence on the behaviour of the sand–rubber mixtures, as the differences in particle origin and type of the two sands are expected to be the dominant factors in assessing the behaviour of the mixtures, as will be discussed later in the paper. Note that the grading curve of CDV was measured after the sample had been compacted in the mould, when some small amount of particle crushing would have been encountered during the preparation method.

Both host sands were mixed with granulated rubber at 20% by mixture dry mass; for a limited number of tests, CDV was also mixed with 10% rubber. A content of rubber of 20% by weight (corresponding to roughly 35–40% by volume) was chosen so that the mixtures would have a behaviour

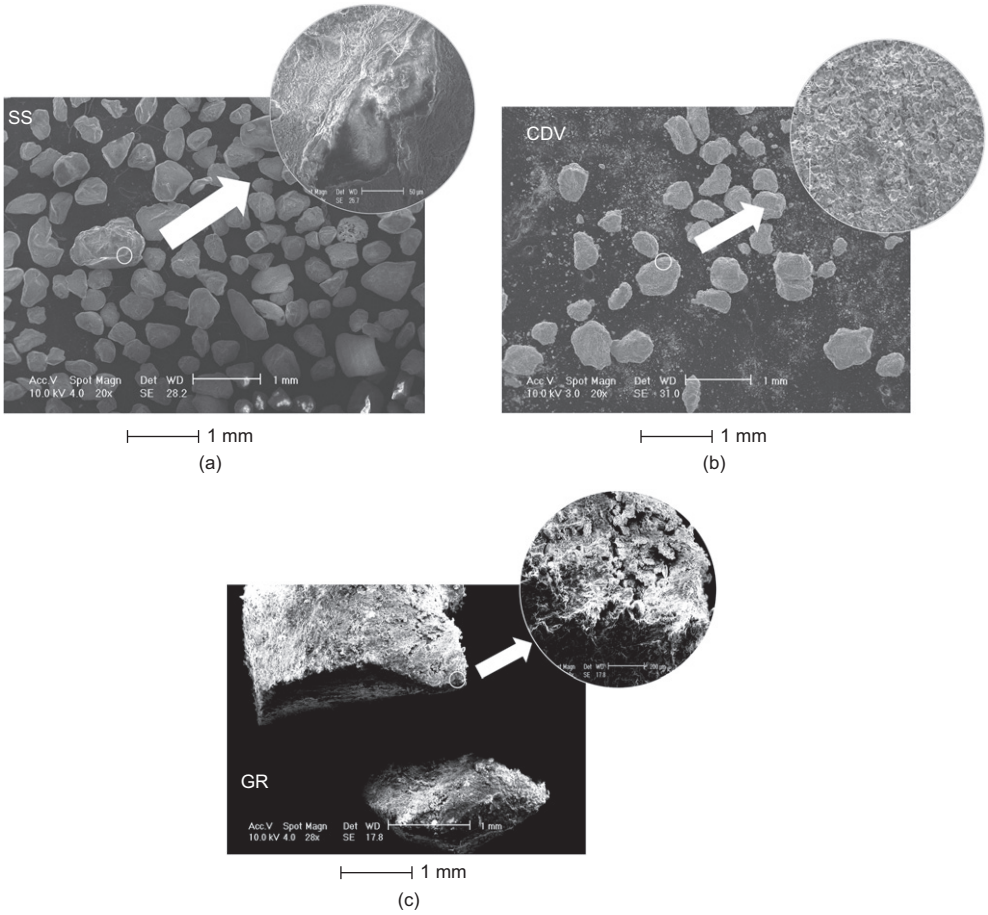

Fig. 1. SEM images of (a) Sydney sand (SS); (b) completely decomposed volcanic rock (CDV) and (c) granulated rubber (GR) and details of surface textures

Table 1. Description of host sands and rubber

Material ID	D_{50}: mm	G_s	C_u
SS	0·32	2·65	1·45
CDV	0·41	2·60	2·45
GR	1·77	1·10	1·31

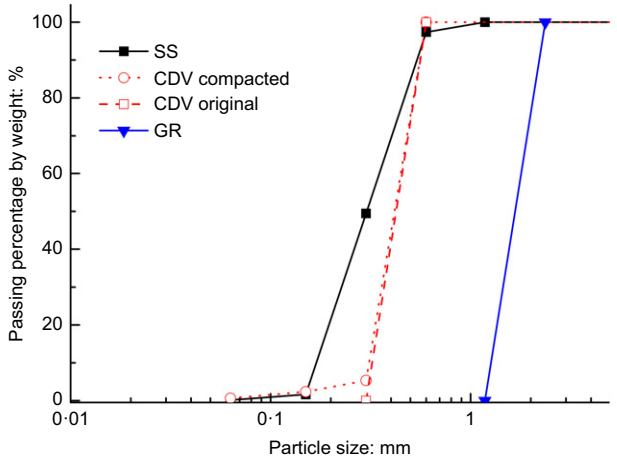

Fig. 2. Grading curves of host sands and granulated rubber

somewhere between sand-like and rubber-like, and the sand portion would have a significant contribution in the response of the specimens (Zornberg *et al.*, 2004; Kim & Santamarina, 2008; Li *et al.*, 2019b). This percentage may also be expected to be representative in engineering practice for soil–recycled shredded tyres (or rubber) mixtures. For simplicity, the specimens of pure CDV, pure Sydney sand and their rubber mixtures are termed CDVR00 (pure CDV sample), SSR00 (pure Sydney sand), CDVR10 (CDV reinforced by rubber at 10% by weight), CDVR20 (CDV reinforced by rubber at 20% by weight) and SSR20 (Sydney sand reinforced by rubber at 20% by weight), respectively, in the figures and subsequent discussions.

Testing apparatus, sample preparation and testing programme

Bender element tests were carried out using two stress-path triaxial testing apparatuses. The first apparatus is of the Bishop and Wesley type (denoted as the B–W type). This system accommodates samples of 50 mm dia. and 100 mm high, and houses a pair of T-shaped lateral bender elements. The second apparatus (denoted as the GDS type) accommodates samples of 76 mm dia. and 152 mm high, and houses a pair of single-tip bender elements.

For both apparatuses used, the bender element inserts were mounted at the middle height of the sample. Schematic diagrams of the bender element configurations for the two stress-path triaxial apparatuses are given in Fig. 3. Note that the T-shaped bender elements (Fig. 3(a)) can be used in measurements of both G_{hh} and G_{hv} at the same time on one sample. The single-tip bender elements used in the GDS-type apparatus (Fig. 3(b)) can measure only G_{hh} or G_{hv} at a given time, depending on the way the bender elements are configured, which means that a full set of G_{hh} and G_{hv} must be measured separately on two different samples. In this case, two samples of the same material type to be tested under the same stress states were prepared at similar void ratios, but the initial conditions of the two samples may not be the same.

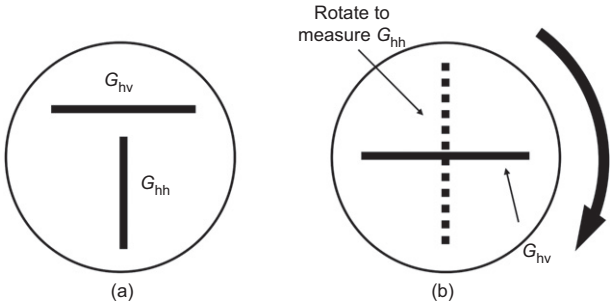

Fig. 3. Schematic configurations of (a) B–W type and (b) GDS type bender elements

The specimens of CDV and its rubber mixtures were prepared in a dry state using the under-compaction method (Ladd, 1978) and were tested in a dry condition, whereas the Sydney sand and its mixtures with rubber were prepared in a moist state and were tested in a fully saturated condition. Note that for the Sydney sand and its mixtures with rubber, no differences would be expected between dry and fully saturated specimens in terms of stiffness and the stiffness–creep relationship. The specimens were prepared in many layers of equal dry (or moist) mass. Each layer was compacted and the whole process was carefully monitored to avoid, as far as possible, particle segregation. During the tests, the radial and axial strains of the dry samples were measured using a set of radial strain gauges (developed by Ackerley *et al.* (2016)) and an external displacement transducer, respectively. The volumetric strain was calculated as $\varepsilon_v = \varepsilon_a + 2 \times \varepsilon_r - \varepsilon_r^2[1 - \varepsilon_a + 2(\varepsilon_a/\varepsilon_r)]$ (Todisco, 2016). For the fully saturated samples, the volumetric strain was estimated based on the volume of expelled water, as recorded by a water volume controller connected to the specimen.

The specimens were subjected to four different stress paths (one isotropic and three anisotropic stress paths), in which both confining stress and deviatoric stress increased at a rate of 5 kPa/min. The applied stress paths are shown as solid points in Fig. 4. The isotropic stress path (denoted as 'ISO') reached a stress state of $p' = \sigma'_a = \sigma'_r = 250$ kPa. For one of the three anisotropic stress paths (conventional shearing path 1, denoted as 'SP1'), the deviatoric stress was applied after an initial stage of isotropic compression at $p' = \sigma'_a = \sigma'_r = 167$ kPa to reach a stress state as $p' = q = 250$ kPa. The anisotropic loadings of stress path 2 (constant p' shearing

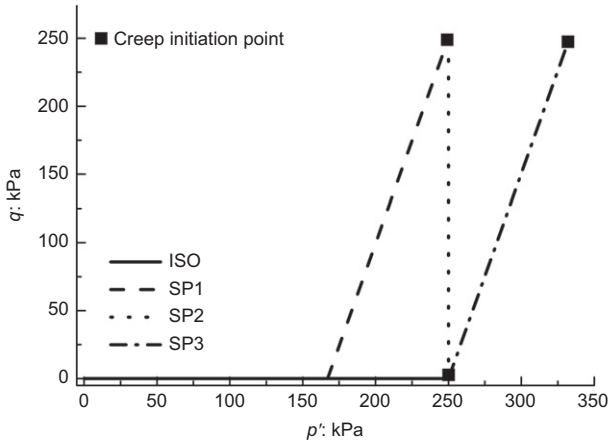

Fig. 4. Different stress paths applied in the study and their abbreviations

path 2, denoted as 'SP2') and stress path 3 (conventional shearing path 3, denoted as 'SP3') were initiated at $p' = \sigma'_a = \sigma'_r = 250$ kPa, but their final stress states were (*a*) $p' = q = 250$ kPa and (*b*) $p' = 333{\cdot}3$ kPa, $q = 250$ kPa, respectively. The strain localisation is believed not to significantly affect the wave transmission under the modest level of stress anisotropy. Creep tests were initiated at the endpoint of each stress path and the applied stress was held for approximately 72 h (3 days). This period of time could be considered as adequate to plot in semi-log scale stiffness against the duration of constant confinement to estimate the rate of stiffness increase (Jovičić & Coop, 1997; Wang & Tsui, 2009; Anastasiadis *et al.*, 2012a). The stiffness, axial strain and volumetric strain were recorded at predetermined time intervals during the 3 days of creep, to quantify the relationship between stiffness and duration of the constant confining pressure, in order to investigate the creep behaviour of the specimens. The application of these four different stress paths was intended to: (*a*) examine creep and the role of isotropic/anisotropic stress state by comparing stress path 'ISO' with 'SP2'; (*b*) examine the role of the stress path, based on comparisons between 'SP1' and 'SP2'; (*c*) examine the influence of the stress ratio on the stiffness–creep behaviour of the samples, comparing stress paths 'SP2' and 'SP3'.

The initial conditions of each test are given in Table 2. The name of each test follows the sequence of 'host material'_'-rubber weight fraction'_'stress path'_'duration of constant confinement'. For example, the name 'SS_R20_ISO_D3' indicates that 'Sydney sand (SS) was mixed with 20% of rubber by weight (R20) and was loaded along an isotropic stress path (ISO) with application of constant confinement for 3 days (D3)'. e_{eq} in Table 2 denotes the equivalent or 'granular' void ratio (first introduced by Feng & Sutter (2000) for sand–rubber mixtures). The equivalent void ratio is given from equation (1)

$$e_{eq} = \frac{V_{rubber} + V_{void}}{V_{sand}} \tag{1}$$

In equation (1), V_{rubber}, V_{void} and V_{sand} denote the volume of rubber, voids and sand grains, respectively.

The input wave and typical output waves from the bender element tests are illustrated in Fig. 5. G_{max} was then calculated by equation (2)

$$G_{max} = \rho V_S^2 \tag{2}$$

where ρ denotes the density of the sample; V_S denotes the velocity of horizontally propagated shear waves picked by the first time of arrival method. Values of G_{hh} and G_{hv} can be determined by measuring the shear wave velocity in different directions as V_{hh} and V_{hv}, accordingly.

Different methods of calculating ρ were employed in equation (2), depending on the testing conditions of the samples. For dry samples, dry bulk density was used in the calculations. For specimens tested under fully saturated conditions, the equivalent density can give higher reliability than bulk density when measuring G_{max} (Youn *et al.*, 2008; Qiu *et al.*, 2015). In this study, equation (3) proposed by Youn *et al.* (2008) was employed to calculate the equivalent density of fully saturated specimens

$$\rho_{eq} = (1 - n)\rho_g + n \times \left(1 - \frac{1}{a}\right)\rho_f \tag{3}$$

where ρ_g and ρ_f denote the density of grains and fluid, respectively. n is the porosity of the sample. a is an adjusting parameter ranging between 2 and 3 (Stoll, 1979) and is taken as 3 in the current study, although it is noticed that its influence on stiffness is small. For the application of the mixture containing synthetics, ρ_g was determined by the effective density of rubber and sand (Li *et al.*, 2017), as given by equation (4)

$$\rho_g = \frac{M_{sand} + M_{rubber}}{V_{sand} + V_{rubber}} \tag{4}$$

where M_{sand}, V_{sand} and M_{rubber}, V_{rubber} denote the mass and volume of sand and rubber, respectively.

Table 2. Bender element testing programme and sample details

Code name of sample	Material	Stress path	G_{max}	e_0	Size: mm	e_{eq}
SS_R00_ISO_D3	SSR00	ISO	$G_{hh} + G_{hv}$	0·85	100 × 50	0·85
SS_R00_SP1_D3	SSR00	SP1	$G_{hh} + G_{hv}$	0·81	100 × 50	0·81
SS_R00_SP2_D3	SSR00	SP2	$G_{hh} + G_{hv}$	0·82	100 × 50	0·82
SS_R00_SP3_D3	SSR00	SP3	$G_{hh} + G_{hv}$	0·89	100 × 50	0·89
SS_R20_ISO_D3	SSR20	ISO	G_{hv}	0·63	152 × 76	1·60
	SSR20	ISO	G_{hh}	0·62	152 × 76	1·60
SS_R20_SP1_D3	SSR20	SP1	G_{hv}	0·60	152 × 76	1·58
	SSR20	SP1	G_{hh}	0·62	152 × 76	1·59
SS_R20_SP2_D3	SSR20	SP2	G_{hv}	0·65	152 × 76	1·65
	SSR20	SP2	G_{hh}	0·66	152 × 76	1·66
SS_R20_SP3_D3	SSR20	SP3	G_{hv}	0·66	152 × 76	1·66
	SSR20	SP3	G_{hh}	0·60	152 × 76	1·58
CDV_R00_ISO_D3	CDVR00	ISO	$G_{hh} + G_{hv}$	1·46	100 × 50	1·46
CDV_R00_SP1_D3	CDVR00	SP1	$G_{hh} + G_{hv}$	1·56	100 × 50	1·56
CDV_R00_SP2_D3	CDVR00	SP2	$G_{hh} + G_{hv}$	1·48	100 × 50	1·48
CDV_R00_SP3_D3	CDVR00	SP3	$G_{hh} + G_{hv}$	1·63	100 × 50	1·63
CDV_R20_ISO_D3	CDVR20	ISO	G_{hv}	1·02	152 × 76	2·21
	CDVR20	ISO	G_{hh}	0·98	152 × 76	2·15
CDV_R20_SP1_D3	CDVR20	SP1	G_{hv}	0·77	152 × 76	1·82
	CDVR20	SP1	G_{hh}	0·83	152 × 76	1·91
CDV_R20_SP2_D3	CDVR20	SP2	G_{hv}	0·79	152 × 76	1·85
	CDVR20	SP2	G_{hh}	0·80	152 × 76	1·87
CDV_R20_SP3_D3	CDVR20	SP3	G_{hv}	0·85	152 × 76	1·92
	CDVR20	SP3	G_{hh}	0·91	152 × 76	2·05
CDV_R10_SP3_D3	CDVR10	SP3	G_{hv}	1·05	152 × 76	1·59
	CDVR10	SP3	G_{hh}	1·04	152 × 76	1·57

RESULTS AND DISCUSSION

Influence of creep on G_{max} of host sands

Plots of G_{hh} and G_{hv} against the duration of constant confinement for the 3 day creep measurements (4320 min) for pure Sydney sand are represented by the open squares in Fig. 6. The results suggest that the SSR00 sample has a negligible stiffness anisotropy when bender element measurements are carried out under the isotropic stress state and that the influence of creep is relatively small for the Sydney sand. It is also seen that the values of G_{hv} are approximately 20% higher than G_{hh} values, when the specimens are subjected to stress anisotropy.

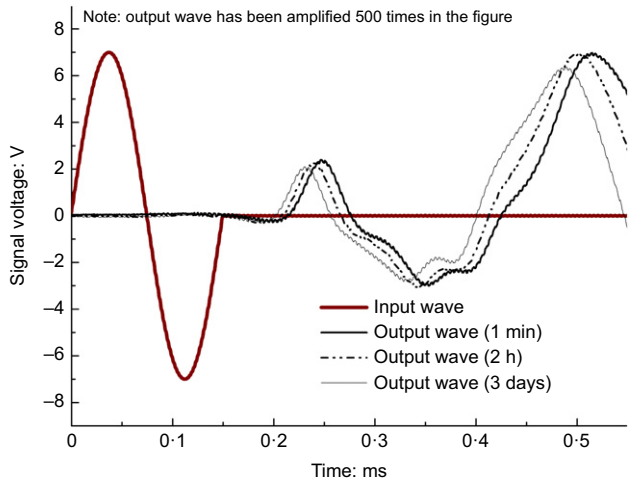

Fig. 5. Typical input and output waves against time during the application of constant confinement

The corresponding results of stiffness against the duration of constant confinement for CDVR00 are shown in Fig. 7. Comparing the data between Figs 6 and 7, it can be observed that the weathered volcanic sand has approximately 30% lower values of stiffness compared with Sydney sand. This lower stiffness is partly ascribed to the intrinsically higher void ratio of the CDV specimens. It is possible that the reduction of stiffness is also contributed by the lower particle strength and softer contacts between CDV particles compared with that of quartz grains (Sandeep & Senetakis, 2017; Sandeep *et al.*, 2018). However, the stiffness of CDVR00 increases at a faster rate than that of SSR00 specimens during the creep stage. For G_{max} of all stress paths, creep increments are linearly proportional to the logarithm of time and at the completion of the long-term loading, the largest stiffness increment is found in the isotropic case, in which both G_{hh} and G_{hv} increased, approximately, by 12%.

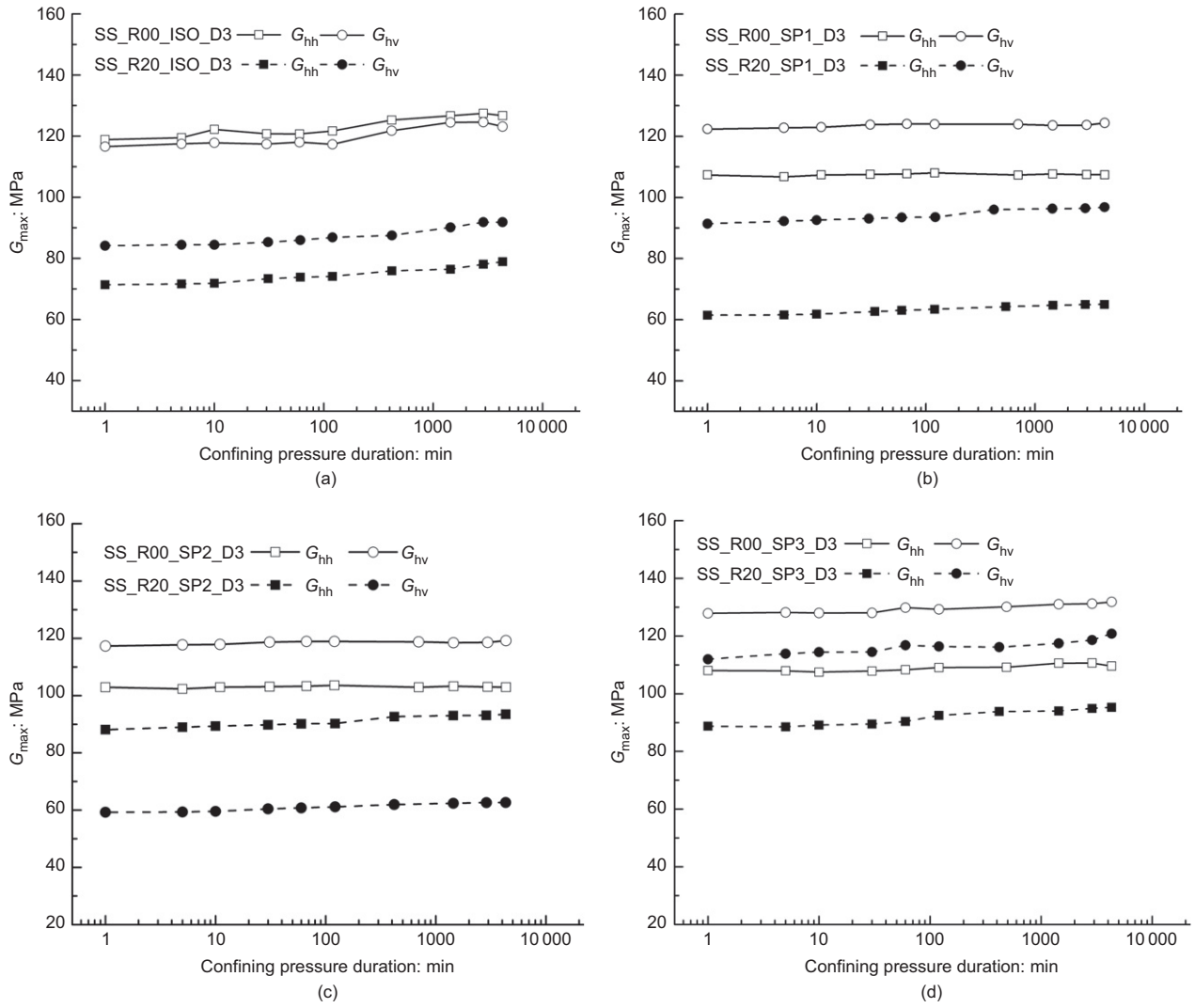

Fig. 6. Influence of duration of constant confinement on G_{max} of pure Sydney sand (SSR00) and its rubber mixture (SSR20) under (a) ISO; (b) SP1; (c) SP2 and (d) SP3 stress paths

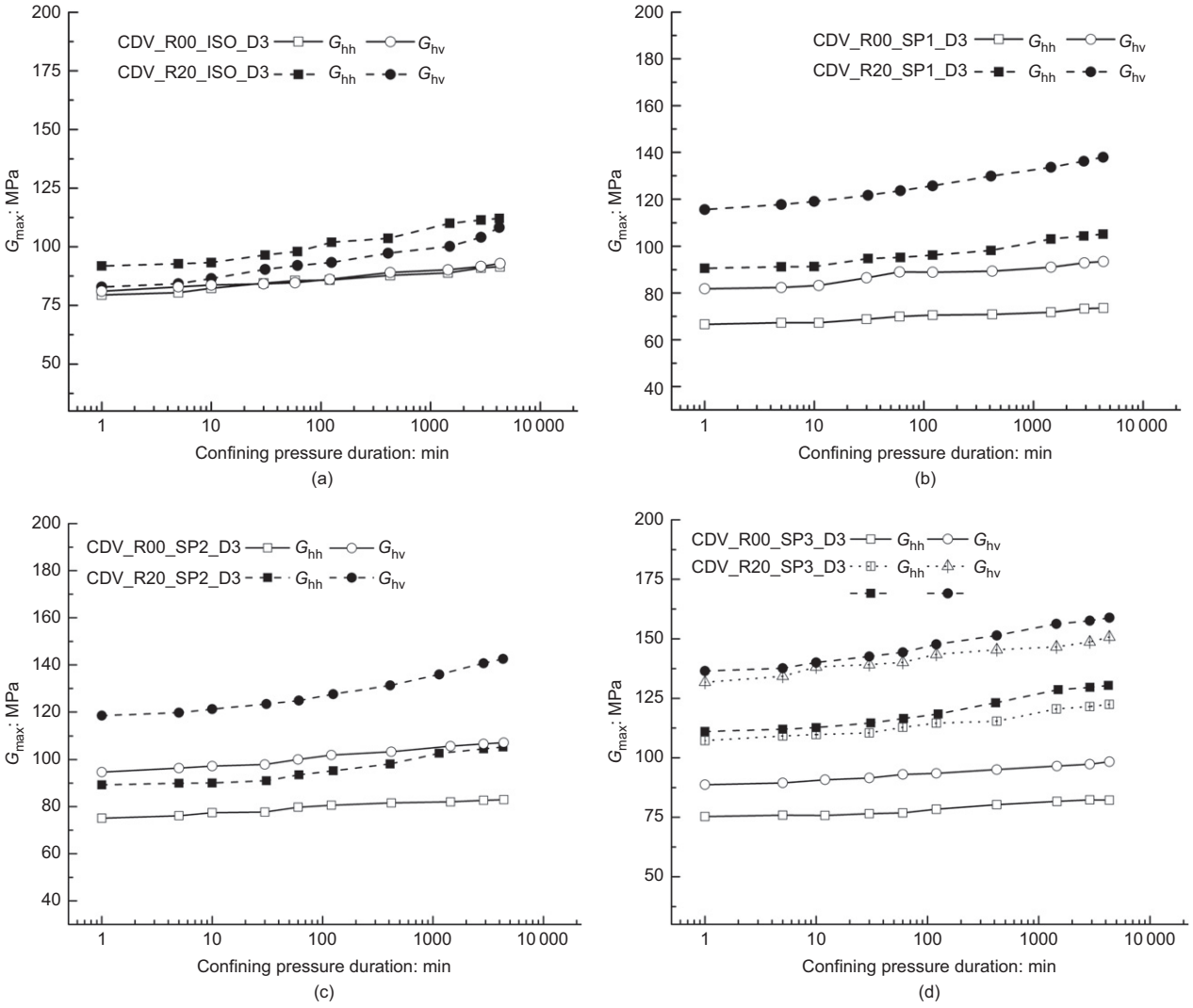

Fig. 7. Influence of duration of constant confinement on G_{max} of pure CDV (CDVR00) and its rubber mixtures (CDVR10 and CDVR20) under (a) ISO; (b) SP1; (c) SP2 and (d) SP3 stress paths

Influence of creep on G_{max} of sand–rubber mixtures

The variation of G_{max} against time of confinement for SSR20 is plotted with the solid markers in Fig. 6. As rubber inevitably participates in the force transmission, both G_{hh} and G_{hv} of all stress paths of SSR20 are lower than those of SSR00. The percentage of stiffness reduction ranges from 15 to 40%, depending on the stress states applied on the specimens. The influence of the inclusion of rubber on G_{max}, from a qualitative standpoint, is in agreement with previous works (Feng & Sutter, 2000; Anastasiadis *et al*., 2012a, 2012b; Lopera Perez *et al*., 2017b). However, G_{hh} and G_{hv} values of SSR20 increased notably for all the different stress paths under the 3 day creep measurements, so that the differences between the stiffness values of SSR00 and SSR20 are much smaller after 3 days of continuous applied stress. These results suggest that the addition of rubber to the quartz sand will reduce G_{max} in the first place, but adverse effects are gradually minimised during the service of an infrastructure/geo-system.

In contrast to the observations on quartz sand–rubber mixtures, it is seen in Fig. 7 that G_{max} values of all cases for CDVR10 and CDVR20 increase when compared with the results for pure CDV, and that the stiffness values of the mixtures with 10% and 20% of rubber are very close. The reinforcement effects are more distinct under the anisotropic stress state. Although most of the studies reported a reduction in G_{max} after the inclusion of rubber, cases of increased stiffness after rubber is added have also been reported (Kim & Santamarina, 2008; Li *et al*., 2016; Lopera Perez *et al*., 2016). The reversed trends observed between CDVR20 and SSR20 suggest that the influence of the inclusion of rubber is highly dependent on the type of host sand. The more distinct reinforcement effects of rubber when added to the crushable sand under anisotropic stress paths compared with the isotropic stress state could be explained, partly, by the hypothesis of increased rigidity of the rubber particles after significant deformations have taken place (Kim & Santamarina, 2008; Li *et al*., 2016). The reinforcement influence of the rubber inclusion is further amplified because of creep. The largest increment is seen in G_{hv} for the ISO case, where the value has increased by 30%, from 83 to 108 MPa. The results suggest that the inclusion of rubber in CDV not only provides higher G_{max}, but also contributes to a more pronounced increase of stiffness with time.

Quantification of G_{max} increment: N_G values

The stiffness increment within 72 h creep duration can be extended to a longer period using the index N_G proposed by Anderson & Stokoe (1978), which quantifies how significant the magnitude of stiffness increment rate

is to the initial stiffness. The expressions are given in equations (5) and (6)

$$I_G = \frac{\Delta G}{\log_{10}(t_2/t_1)} \tag{5}$$

$$N_G = \frac{I_G}{G_{t_1}} \tag{6}$$

Table 3. N_G values of each material under various stress paths

Tests types	ISO: %	SP1: %	SP2: %	SP3: %
SSR00				
G_{hh}	1·8	0·0	0·2	0·4
G_{hv}	1·5	0·5	0·6	0·9
SSR20				
G_{hh}	2·5	1·5	3·1	2·1
G_{hv}	2·9	1·7	3·9	2·2
CDVR00				
G_{hh}	4·2	2·9	2·9	2·5
G_{hv}	4·0	3·9	3·6	3·0
CDVR20				
G_{hh}	6·2	4·4	4·9	4·1
G_{hv}	8·4	5·1	5·6	4·5
CDVR10				
G_{hh}	—	—	—	3·4
G_{hv}	—	—	—	4·0

where ΔG is the stiffness increment during the study period; t_2 is equal to the end time of loading (min); t_1 is the reference time; and G_{t_1} denotes the stiffness at time t_1. Larger N_G values represent a more significant stiffness increment in the service period.

It is noted that the preceding equations were originally introduced in the study of G_{max} of clays in which the reference time t_1 was selected at 1000 min to ensure that any variations of soil properties were not triggered by the consolidation. In the present study, the materials are highly permeable and it is more reasonable to assume that the consolidation is completed immediately after reaching the target stress state. Thus, t_1 was selected as 1 min. Based on the analysis of the data, a summary of the N_G values is given in Table 3.

Based on the results in Table 3, it can be concluded that, for all the combinations of material type (i.e. SSR00, SSR20, CDVR00, CDVR20, CDVR10) and stress paths (i.e. ISO, SP1, SP2, SP3), the highest N_G values were observed for the isotropic stress path ('ISO' case). The only exemption was noticed for SSR20, which material type had the highest N_G values for the anisotropic stress path SP2, with the isotropic stress path giving the second highest values. The different stress paths (SP1 and SP2) did not add any differences to the stiffness–creep relationship, yet a larger stress ratio (q/p') contributes to more distinct differences in the N_G values between G_{hv} and G_{hh}. For measurements of stiffness under isotropic stress paths, the N_G values of pure CDV were two to three times higher compared with that of the pure Sydney sand. The rubber inclusion magnified N_G values of both

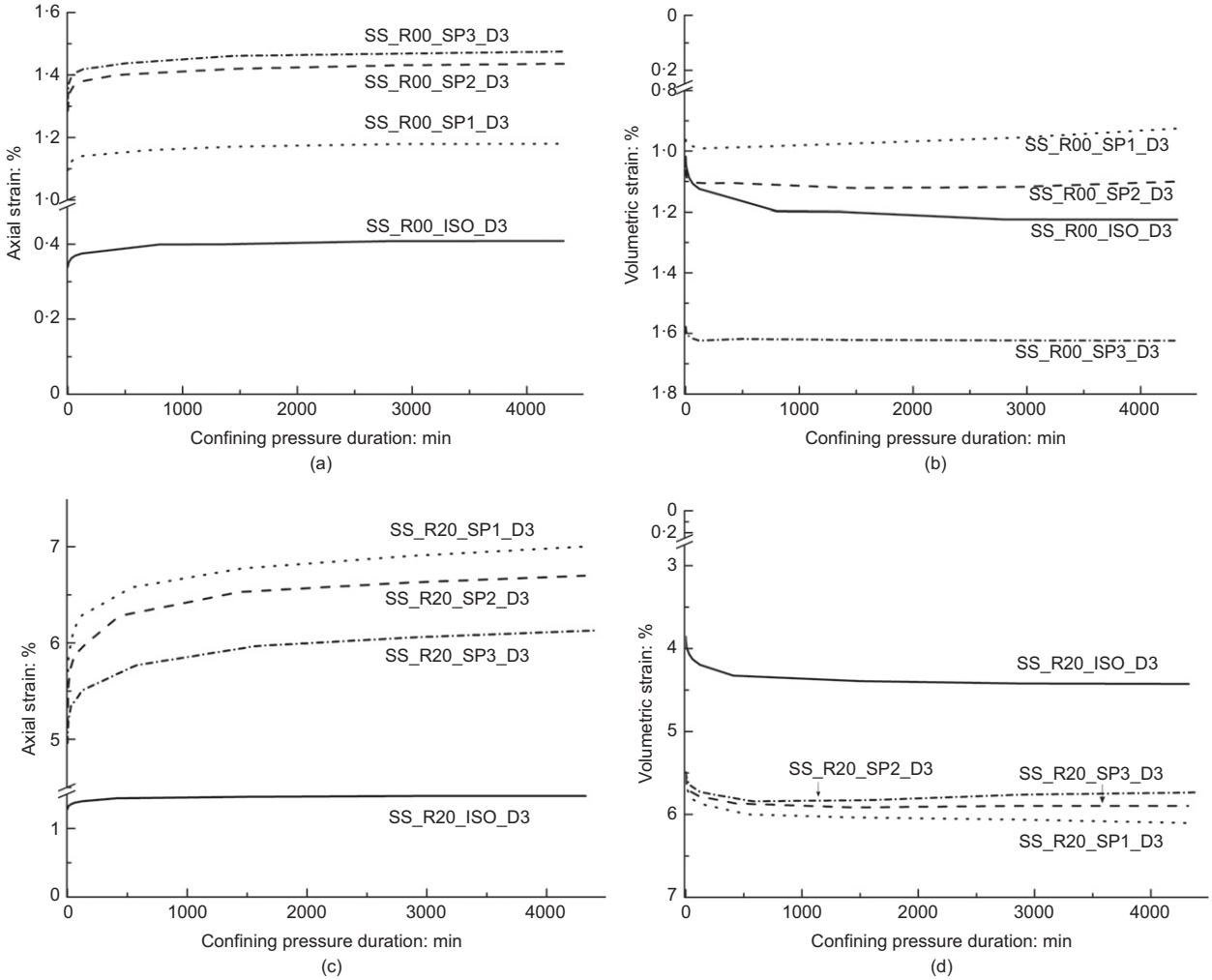

Fig. 8. Representative (a) axial strain and (b) volumetric strain of SSR00; (c) axial strain and (d) volumetric strain of SSR20

Sydney sand and CDV, and the most important influence of creep on stiffness was observed for sample CDVR20. Although sample CDVR10 has G_{max} values that are close to those of CDVR20, the N_G values for 10% rubber locate between that of CDVR00 and CDVR20. These data suggest that the influence of creep on stiffness is more significant for crushable sands and the addition of rubber magnifies creep effects when compared with pure sands.

The data in Table 3 also suggest that N_G values of G_{hh} are lower than those of G_{hv} under the anisotropic stress states for most of the specimens. Based on the study by Gao *et al.* (2012), the preceding observations could, partly, be ascribed to the microscopic mechanism whereby breakdown arching effects progressively weaken the horizontal strong forces in the assemblies, yet strong forces along the axial directions continuously increase. As a result, G_{hv} always increased faster than G_{hh} under the application of anisotropic stress state. The process can also be reflected in the response of strains, which is discussed in the next section.

Creep deformations

Figures 8 and 9 present the deformations of the specimens subjected to creep. The interval on the vertical axis of each plot represents the strain during the consolidation stage. It is observed for SSR00 in Figs 8(a) and 8(b) that axial and volumetric strains during consolidation are very low in magnitude at all the selected stress states. During the creep stage, negligible variations of axial and volumetric strains are also observed for all the SSR00 specimens, and the data in Figs 9(a) and 9(b) would suggest that the specimens of CDVR00 are more compressive than those of SSR00.

It is also found, based on the data shown in Figs 8(c), 8(d) and 9(c), 9(d), that the inclusion of rubber increases the compressibility (in terms of greater consolidation and creep deformations) of the specimens compared with that of the host sands, which has also been recorded in previous works (Fu *et al.*, 2014, 2017). It is also seen for all materials that anisotropic cases exhibit lower variation of volumetric strain during creep, when compared to the isotropic cases. Larger variation of volumetric strain during creep not only indicates larger adjustments in the void ratio to which the empirical expressions of G_{max} are directly linked (Hardin & Richart Jr., 1963; Hardin & Black, 1966), but also implies that more dynamic fabric evolutions have taken place during the period of application of constant confining pressure. These results indicate that the time effects on G_{max} differ from those on other properties; according to the previous works, more drastic time effects on the shearing rate (Augustesen *et al.*, 2004; Kwok & Bolton, 2010) and particle breakage (Chen & Zhang, 2016) would take place under larger anisotropic stress states, while G_{max} showed the opposite trend, in which the most pronounced stiffness increment was observed for the specimens undergoing the isotropic confining pressure.

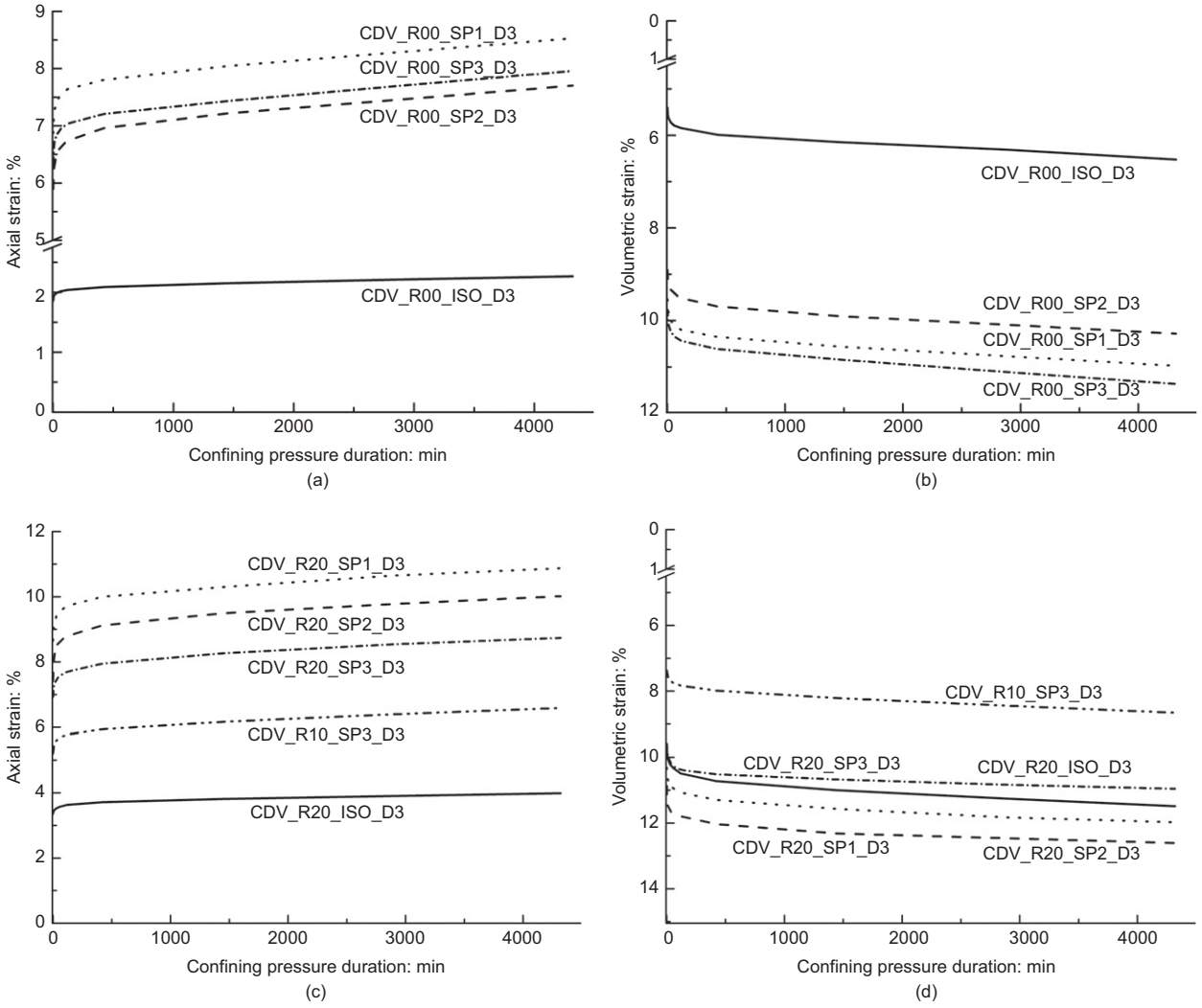

Fig. 9. Representative (a) axial and (b) volumetric strain of CDVR00; (c) axial and (d) volumetric strain of CDVR10 and CDVR20

Variations in stiffness anisotropy

Stiffness anisotropy can be quantified by the ratio of G_{hh} over G_{hv}. In order to eliminate, as far as possible, the influences of different void ratios, the G_{max} values of SSR20 and CDVR20 were normalised with respect to a void ratio function during the creep, as shown in equation (7). The void ratio function $f(e)$ proposed by Jamiolkowski *et al.* (1991) and presented in equation (8) was adopted for the normalisation

$$G^{Nor} = \frac{G_{max}}{f(e)} \tag{7}$$

$$f(e) = e^{-1.3} \tag{8}$$

In equation (7), G^{Nor} is the normalised shear stiffness, which can be considered as G_{hh}^{Nor} or G_{hv}^{Nor}. Thus, the stiffness anisotropy of pure sand and sand–rubber mixtures is presented as G_{hh}/G_{hv} and $G_{hh}^{Nor}/G_{hv}^{Nor}$, respectively.

The variation of stiffness anisotropy for the different specimens is shown in Figs 10(a) and 10(c). At first sight, both specimens of SSR00 and CDVR00 show negligible inherent anisotropy under the isotropic stress state. During the measurements at the creep stage under isotropic loading, the stiffness anisotropy for CDVR00 and SSR00 does not change noticeably because of the similar magnitude of stiffness increments for both G_{hh} and G_{hv}. Under stress anisotropy, G_{hv} is much larger than the corresponding G_{hh} values for both SSR00 and CDVR00 samples, as stress-induced anisotropy dominates their behaviour. As G_{hv} increases more quickly than G_{hh}, this induces further stiffness anisotropy to the samples.

The data in Figs 10(b) and 10(d) also suggest that the inherent stiffness anisotropy prior to creep has greatly changed after the inclusion of rubber to both host sands. For SSR20 specimens, G_{hh} reduced more markedly than G_{hv}, which resulted in lower $G_{hh}^{Nor}/G_{hv}^{Nor}$ values compared to those of SSR00 at all stress states. This observation implies that, for Sydney sand, the stiffness anisotropy has been magnified after rubber was added. Contrary to SSR20, the stiffness anisotropy $G_{hh}^{Nor}/G_{hv}^{Nor}$ for CDVR20 in Fig. 10(d) has increased to around 1·1. For anisotropic cases, although CDVR20 samples have become more 'nominally isotropic' (i.e. $G_{hh}^{Nor}/G_{hv}^{Nor}$ ratios are closer to 1 compared with the corresponding values of CDVR00 under the given stress state) than those of CDVR00, $G_{hh}^{Nor}/G_{hv}^{Nor}$ ratios have also been more sensitive to the variation of stress anisotropy after rubber was added, when considering the inherent anisotropy of the sample ($G_{hh}^{Nor}/G_{hv}^{Nor} \approx 1{\cdot}1$).

Examinations of particle crushing of the specimens after the completion of creep tests

The solid lines 'ISO_D3', 'SP1_D3', 'SP2_D3' and 'SP3_D3' presenting the post-testing grading curves of each test at different stress states are plotted in Fig. 11(a). Additional tests subjected to the corresponding stress states without the creep stage are defined as 'fast tests'. Details of the 'fast tests' are listed in Table 4 and their corresponding

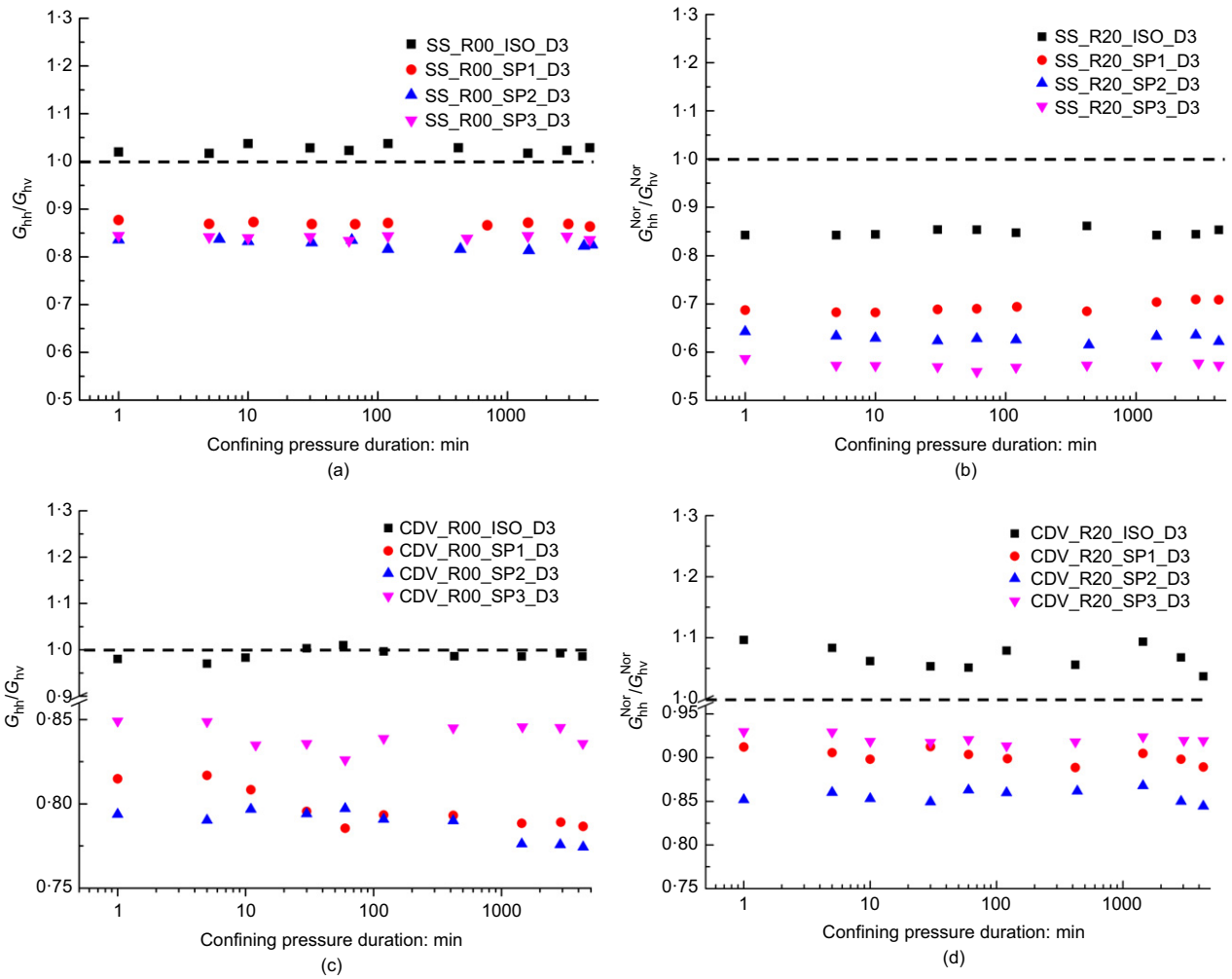

Fig. 10. Variation of stiffness anisotropy of (a) SSR00; (b) SSR20; (c) CDVR00 and (d) CDVR20

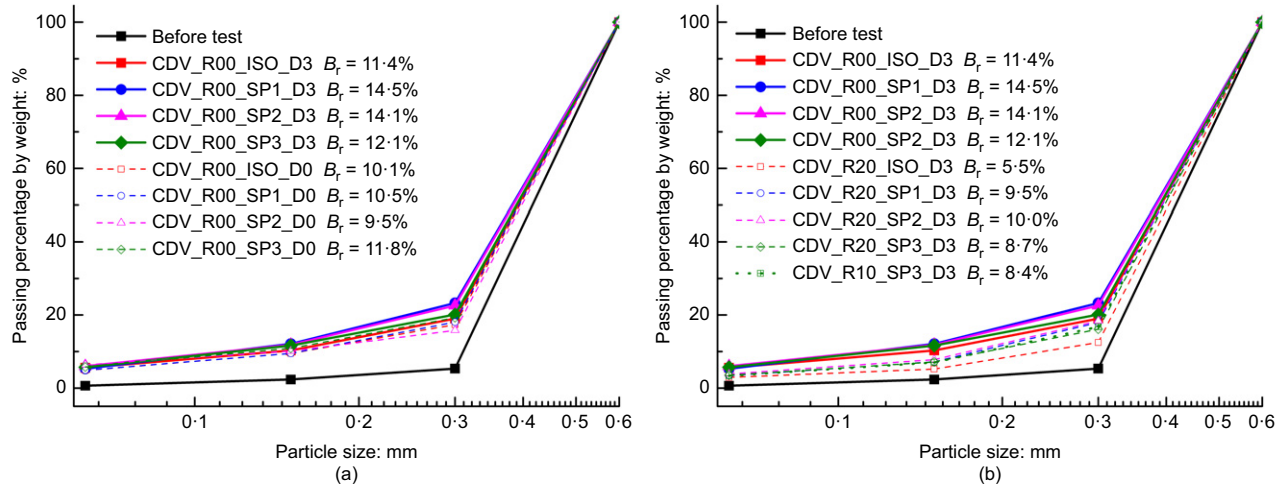

Fig. 11. Post-testing sieving results of (a) CDVR00 and (b) CDVR10 and CDVR20

Table 4. Details of fast tests and long-term tests in breakage analysis

Tests name	Materials	e_0	Stress path	Durations
CDV_R00_ISO_D0	CDVR00	1·44	ISO	0 min
CDV_R00_ISO_D3	CDVR00	1·46	ISO	3 days
CDV_R00_SP1_D0	CDVR00	1·55	SP1	0 min
CDV_R00_SP1_D3	CDVR00	1·56	SP1	3 days
CDV_R00_SP2_D0	CDVR00	1·44	SP2	0 min
CDV_R00_SP2_D3	CDVR00	1·48	SP2	3 days
CDV_R00_SP3_D0	CDVR00	1·59	SP3	0 min
CDV_R00_SP3_D3	CDVR00	1·63	SP3	3 days

post-testing sieving results are represented by the dashed lines 'ISO_D0', 'SP1_D0', 'SP2_D0' and 'SP3_D0' in Fig. 11(a). Based on the grading curves in Fig. 11(a), the more enhanced levels of particle breakage are found in the long-term tests, verifying that particle breakage within CDVR00 has been further developed under a 3 day confinement. Fig. 11(b) presents post-testing grading curves of CDVR20 and CDVR00 for creep tests. It can be observed that the rubber inclusion noticeably mitigates particle breakage for all stress paths, which shows agreement with published data in the literature (Fu *et al.*, 2015; Li *et al.*, 2019a). The legends of Figs 11(a) and 11(b) provide information on the relative breakage (B_r) for each sample calculated from the method proposed by Hardin (1985). For pure CDV, the data indicate B_r values ranging, approximately, from 10% to 15%. Within the scatter of the data, it can be observed that there is an increase of the relative breakage values when the samples are subjected to creep (i.e. codes 'D3' compared with 'D0') and that the values are smaller for the mixtures compared with that of the pure sand.

The above results suggest that the deformations of CDVR00 and CDVR20 discussed in the previous sections originate from very different mechanisms. The plastic particle breakage due to the lower particle strength played a vital role in the increasing soil compressibility and the subsequent soil creep for CDVR00 specimens (Bowman & Soga, 2003; McDowell & Khan, 2003). Although the rubber protection to the weak CDV particles might restrain soil creep, given the breakage is an important mechanism for soil creep (Takei *et al.*, 2001; McDowell, 2003; McDowell & Khan, 2003), CDVR20 still underwent a more significant volumetric strain and stiffness increment than CDVR00, indicating that particle breakage is not the dominating mechanism for the creep of rubber–sand mixtures at the rubber fraction of 20%. Instead, it is the deformation of the soft rubber particles that plays a more important role in the increasing soil compressibility and more pronounced soil creep. It is hypothesised that the large deformations of rubber particles continuously relocate the positions of adjacent particles, leading to the creation of new contacts so as to redistribute the stresses. For the rubber contents used in the current study (20% as benchmark content and additionally 10% for a limited number of tests), the preceding process seems to be sufficiently intense to compensate for the diminished 'chained-event' (i.e. repetitive cycles of 'crushing–particle rearrangement–stress distribution–crushing', verified by Takei *et al.* (2001), are restrained due to less particle breakage). The fabric evolutions triggered by such mechanisms can be further developed and result in aggravating soil stiffening effects under long-term constant applied stress; this dominates soil creep of sand–rubber mixtures and overwhelms the original creep mechanism of the host sand (i.e. sand particle micro-adjustment for SSR00 and soil particle breakage for CDVR00).

CONCLUSIONS

The small-strain stiffness of two types of uniformly graded sands, namely Sydney sand (SSR00) and completely decomposed volcanic rock (CDVR00), as well as their rubber mixtures (SSR20, CDVR10 and CDVR20), was investigated by performing bender element tests in stress path triaxial apparatus. The study focused on the relationship between G_{max} and the duration of constant confinement, for a period of 3 days, applying isotropic and anisotropic stress paths to the specimens. The major conclusions from the study are summarised below.

(*a*) The influence of the inclusion of rubber on the stiffness of the mixture depended, predominantly, on the type of host sand. For Sydney sand, the small-strain stiffness significantly decreased after rubber was added, but for CDV, a clear increase of stiffness was observed for the mixtures compared with the pure sand.

(*b*) Specimens of CDV were found to be more susceptible to soil creep than those of Sydney sand. The presence of rubber amplified the influences of creep (i.e. increase of stiffness during measurements at a constant confining pressure) for both sands. The slow, yet continuous deformation of the soft rubber particles under constant

confinement induced more significant fabric changes and resulted in a more pronounced influence of creep on the mixtures compared with that on pure sand.

(*c*) For all the materials studied, G_{hv} increased faster than G_{hh} when the specimens were subjected to anisotropic stress paths, and the increase of stiffness with the duration of constant confinement was more pronounced for the isotropic stress paths compared with the tests under anisotropic loading. These observations could be partly explained by or linked to the smaller variations of the volumetric strain during creep measurements under anisotropic stress states.

(*d*) The increased grain breakage of CDVR00 is associated with the more pronounced stiffness increment. However, the post-testing sieving analysis on CDV–rubber mixtures suggested that rubber-induced deformations rather than particle crushing is the dominating factor affecting the relationship of stiffness–time at a rubber fraction of 20%. As a result, specimens of CDVR20 appeared to be more significantly affected by creep phenomena, even though the specimens had less grain breakage.

ACKNOWLEDGEMENTS

The study was fully supported by grants from the Research Grant Council of Hong Kong Special Administrative Region (HKSAR), China (project no. CityU 11210419 and project no. CityU 11206617). The authors would like to acknowledge the Geotechnical Engineering Office (GEO) of the Civil Engineering and Development Department, Hong Kong SAR, for the supply of the weathered volcanic material tested in the study.

NOTATION

C_u	coefficient of uniformity
D_{50}	mean grain size
e_0	initial void ratio
e_1	void ratio when creep stages initiate
e_{eq}	equivalent void ratio
$f(e)$	void ratio function
G_{max}	small-strain stiffness
G_{hh}^{Nor}	G_{hh} normalised by void ratio function
G_{hv}^{Nor}	G_{hv} normalised by void ratio function
G_s	specific gravity
G_{vh}, G_{hh}, G_{hv}	three independent components of small-strain shear stiffness
I_G	slope of stiffness increment in stiffness–log time plane
M_{rubber}	mass of rubber in an assembly
M_{sand}	mass of sand in an assembly
N_G	index quantifying stiffness increment because of creep with respect to a reference stiffness
n	porosity
p'	mean effective confining stress
q	deviatoric stress
V_{hh}	horizontally propagated, horizontally polarised shear wave
V_{hv}	horizontally propagated, vertically polarised shear wave
V_{rubber}	volume of rubber in an assembly
V_{sand}	volume of sand in an assembly
V_{void}	volume of voids in an assembly
ε_a	axial strain
ε_r	radial strain
ε_v	volumetric strain
ρ_{eq}	equivalent density considering influences of liquid
ρ_g	grain density considering the mass of geosynthetics
σ'_a	effective axial stress
σ'_r	effective radial stress

REFERENCES

Ackerley, S., Standing, J. & Hosseini Kamal, R. (2016). A system for measuring local radial strains in triaxial apparatus. *Géotechnique* **66**, No. 6, 515–522, https://doi.org/10.1680/jgeot.15.T.027.

Allen, T. & Bathurst, R. (2002). Observed long-term performance of geosynthetic walls and implications for design. *Geosynth. Int.* **9**, No. 5–6, 567–606.

Anastasiadis, A., Senetakis, K., Pitilakis, K., Gargala, C. & Karakasi, I. (2012a). Dynamic behavior of sand/rubber mixtures, Part I: effect of rubber content and duration of confinement on small-strain shear modulus and damping ratio. *J. ASTM Int.* **9**, No. 2, 1–19.

Anastasiadis, A., Senetakis, K. & Pitilakis, K. (2012b). Small-strain shear modulus and damping ratio of sand–rubber and gravel–rubber mixtures. *Geotech. Geol. Engng* **30**, No. 2, 363–382.

Anderson, D. & Stokoe, K. (1978). Shear modulus: a time-dependent soil property. In *Dynamic geotechnical testing* (eds M. L. Silver and D. Tiedemann), ASTM STP 654, pp. 66–90. West Conshohocken, PA, USA: ASTM International.

ASTM (1998). ASTM D6270-98: Standard practice for use of scrap tires in civil engineering applications. West Conshohocken, PA, USA: ASTM International.

Augustesen, A., Liingaard, M. & Lade, P. V. (2004). Evaluation of time-dependent behavior of soils. *Int. J. Geomech. ASCE* **4**, No. 3, 137–156.

Bernal, A., Salgado, R., Swan, R. & Lovell, C. (1997). Interaction between tire shreds, rubber–sand and geosynthetics. *Geosynth. Int.* **4**, No. 6, 623–643.

Bowman, E. T. & Soga, K. (2003). Creep, ageing and microstructural change in dense granular materials. *Soils Found.* **43**, No. 4, 107–117.

Chen, X. & Zhang, J. (2016). Effect of load duration on particle breakage and dilative behavior of residual soil. *J. Geotech. Geoenviron. Engng* **142**, No. 9, 06016008.

Chow, F., Jardine, R., Brucy, F. & Nauroy, J. (1998). Effects of time on capacity of pipe piles in dense marine sand. *J. Geotech. Geoenviron. Engng* **124**, No. 3, 254–264.

Daramola, O. (1980). Effect of consolidation age on stiffness of sand. *Géotechnique* **30**, No. 2, 213–216, https://doi.org/10.1680/geot.1980.30.2.213.

Edil, T. (ed.) (2012). *Testing and specification of recycled materials for sustainable geotechnical construction*, ASTM STP 1540. West Conshohocken, PA, USA: ASTM International.

Edil, T. B. (2002). Mechanical properties and mass behavior of shredded tire-soil mixtures. In *Proceedings of the international workshop on light-weight geo-materials*, pp. 17–32. Tokyo, Japan: Japanese Geotechnical Society.

Edinçliler, A. & Ayhan, V. (2010). Influence of tire fiber inclusions on shear strength of sand. *Geosynth. Int.* **17**, No. 4, 183–192.

Edinçliler, A. & Cagatay, A. (2013). Weak subgrade improvement with rubber fibre inclusions. *Geosynth. Int.* **20**, No. 1, 39–46.

Fannin, R. (2001). Long-term variations of force and strain in a steep geogrid-reinforced soil slope. *Geosynth. Int.* **8**, No. 1, 81–96.

Feng, Z. Y. & Sutter, K. G. (2000). Dynamic properties of granulated rubber/sand mixtures. *Geotech. Test. J.* **23**, No. 3, 338–344.

Foose, G. J., Benson, C. H. & Bosscher, P. J. (1996). Sand reinforced with shredded waste tires. *J. Geotech. Engng ASCE* **112**, No. 9, 760–767.

Fu, R., Coop, M. & Li, X. (2014). The mechanics of a compressive sand mixed with tyre rubber. *Géotechnique Lett.* **4**, No. 3, 238–243, https://doi.org/10.1680/geolett.14.00027.

Fu, R., Coop, M., Senetakis, K. & Li, X. (2015). An investigation of the particle breakage behaviour of rubber reinforced sand. In *Geomechanics from micro to macro* (eds K. Soga, K. Kumar, G. Biscontin and M. Kuo), pp. 1347–1350. Leiden, the Netherlands: CRC Press/Balkema.

Fu, R., Coop, M. & Li, X. (2017). Influence of particle type on the mechanics of sand–rubber mixtures. *J. Geotech. Geoenviron. Engng* **143**, No. 9, 04017059.

Gao, Y., Wang, Y. H. & Su, J. C. (2012). Mechanisms of aging-induced modulus changes in sand under isotropic and anisotropic loading. *J. Geotech. Geoenviron. Engng* **139**, No. 3, 470–482.

Hardin, B. O. (1985). Crushing of soil particles. *J. Geotech. Engng ASCE* **111**, No. 10, 1177–1192.

Hardin, B. O. & Richart, F. Jr. (1963). Elastic wave velocities in granular soils. *J. Soil Mech. Found. Div. ASCE* **89**, No. SM1, 33–65.

Hardin, B. O. & Black, W. L. (1966). Sand stiffness under various triaxial stresses. *J. Soil Mech. Found. Div. ASCE* **92**, No. SM2, 27–42.

Howie, J., Shozen, T. & Vaid, Y. (2002). Effect of ageing on stiffness of very loose sand. *Can. Geotech. J.* **39**, No. 1, 149–156.

Humphrey, D. N. & Sandford, T. C. (1993). Tire chips as lightweight subgrade fill and retaining wall backfill. In *Proceedings of the symposium on recovery and effective reuse of discarded materials and by-products for construction of highway facilities*, pp. 5–87. Washington, DC, USA: US Department of Transportation, Federal Highway Administration.

Jamiolkowski, M., Leroueil, S. & Lo Presti, D. C. (1991). Design parameters from theory to practice (Theme Lecture). In *Geo-coast 1991: proceedings of international conference on geotechnical engineering for coastal development*, pp. 877–917. Yokosuka City, Japan: Port and Harbour Research Institute.

Jovičić, V. & Coop, M. (1997). Stiffness of coarse-grained soils at small strains. *Géotechnique* **47**, No. 3, 545–561, https://doi.org/10.1680/geot.1997.47.3.545.

Kim, H. K. & Santamarina, J. (2008). Sand–rubber mixtures (large rubber chips). *Can. Geotech. J.* **45**, No. 10, 1457–1466.

Kongkitkul, W., Tatsuoka, F. & Hirakawa, D. (2007). Creep rupture curve for simultaneous creep deformation and degradation of geosynthetic reinforcement. *Geosynth. Int.* **14**, No. 4, 189–200.

Kuhn, M. R. & Mitchell, J. K. (1993). New perspectives on soil creep. *J. Geotech. Engng ASCE* **119**, No. 3, 507–524.

Kwok, C. Y. & Bolton, M. (2010). DEM simulations of thermally activated creep in soils. *Géotechnique* **60**, No. 6, 425–433, https://doi.org/10.1680/geot.2010.60.6.425.

Ladd, R. (1978). Preparing test specimens using undercompaction. *Geotech. Test. J.* **1**, No. 1, 16–23.

Li, B., Huang, M. & Zeng, X. (2016). Dynamic behavior and liquefaction analysis of recycled-rubber sand mixtures. *J. Mater. Civ. Engng* **28**, No. 11, 04016122.

Li, M. N., He, H. & Senetakis, K. (2017). Behavior of carbon fiber-reinforced recycled concrete aggregate. *Geosynth. Int.* **24**, No. 5, 480–490.

Li, W., Kwok, C. Y. & Senetakis, K. (2019a). Effects of inclusion of granulated rubber tyres on the mechanical behaviour of a compressive sand, *Can. Geotech. J.* **57**, No. 5, 763–769.

Li, W., Kwok, C. Y., Sandeep, C. S. & Senetakis, K. (2019b). Sand type effect on the behaviour of sand-granulated rubber mixtures: integrated study from micro-to macro-scales. *Powder Technol.* **342**, No. 15, 907–916.

Liu, H. (2012). Long-term lateral displacement of geosynthetic-reinforced soil segmental retaining walls. *Geotext. Geomembr.* **32**, 18–27.

Lopera Perez, J. C., Kwok, C. & Senetakis, K. (2016). Effect of rubber size on the behaviour of sand–rubber mixtures: a numerical investigation. *Comput. Geotech.* **80**, 199–214.

Lopera Perez, J. C., Kwok, C. Y. & Senetakis, K. (2017a). Micromechanical analyses of the effect of rubber size and content on sand-rubber mixtures at the critical state. *Geotext. Geomembr.* **45**, No. 2, 81–97.

Lopera Perez, J. C., Kwok, C. & Senetakis, K. (2017b). Investigation of the micro-mechanics of sand–rubber mixtures at very small strains. *Geosynth. Int.* **24**, No. 1, 30–44.

McDowell, G. (2003). Micromechanics of creep of granular materials. *Géotechnique* **53**, No. 10, 915–916, https://doi.org/10.1680/geot.2003.53.10.915.

McDowell, G. & Khan, J. (2003). Creep of granular materials. *Granular Matter* **5**, No. 3, 115–120.

Mesri, G., Feng, T. & Benak, J. (1990). Postdensification penetration resistance of clean sands. *J. Geotech. Engng ASCE* **116**, No. 7, 1095–1115.

Ngo, A. T. & Valdes, J. R. (2007). Creep of sand–rubber mixtures. *J. Mater. Civ. Engng* **19**, No. 12, 1101–1105.

Nuntapanich, N., Kongkitkul, W., Tatsuoka, F. & Jongpradist, P. (2018). Prediction of creep behaviour from load relaxation behaviour of polymer geogrids. *Geosynth. Int.* **25**, No. 3, 334–349.

Qiu, T., Huang, Y., Guadalupe-Torres, Y., Baxter, C. D. & Fox, P. J. (2015). Effective soil density for small-strain shear waves in saturated granular materials. *J. Geotech. Geoenviron. Engng* **141**, No. 9, 04015036.

Sandeep, C. S. & Senetakis, K. (2017). Exploring the micromechanical sliding behavior of typical quartz grains and completely decomposed volcanic granules subjected to repeating shearing. *Energies* **10**, No. 3, article 370.

Sandeep, C., Todisco, M., Nardelli, V., Senetakis, K., Coop, M. & Lourenco, S. (2018). A micromechanical experimental study of highly/completely decomposed tuff granules. *Acta Geotech.* **13**, No. 6, 1355–1367.

Senetakis, K. & Anastasiadis, A. (2015). Effects of state of test sample, specimen geometry and sample preparation on dynamic properties of rubber–sand mixtures. *Geosynth. Int.* **22**, No. 4, 301–310.

Senetakis, K., Anastasiadis, A. & Pitilakis, K. (2012). Dynamic properties of dry sand/rubber (SRM) and gravel/rubber (GRM) mixtures in a wide range of shearing strain amplitudes. *Soil Dyn. Earthq. Engng* **33**, No. 1, 38–53.

Stoll, R. D. (1979). Experimental studies of attenuation in sediments. *J. Acoust. Soc. Am.* **66**, No. 4, 1152–1160.

Takei, M., O. Kusakabe, & T. Hayashi (2001). Time-dependent behavior of crushable materials in one-dimensional compression tests. *Soils Found.* **41**, No. 1, 97–121.

Todisco, M. C. (2016). *Behaviour of non-convergent soils: effect of particle size, mineralogy and fabric*. PhD thesis, City University of Hong Kong, Hong Kong, China.

Tsang, H. H. (2008). Seismic isolation by rubber–soil mixtures for developing countries. *Earthq. Engng Struct. Dyn.* **37**, No. 2, 283–303.

Tsiavos, A., Alexander, N. A., Diambra, A., Ibraim, E., Vardanega, P. J., Gonzalez-Buelga &, A. & Sextos, A. (2019). A sand–rubber deformable granular layer as a low-cost seismic isolation strategy in developing countries: experimental investigation. *Soil Dyn. Earthq. Engng* **125**, 105731.

Wang, Y. H. & Gao, Y. (2013). Mechanisms of aging-induced modulus changes in sand with inherent fabric anisotropy. *J. Geotech. Geoenviron. Engng* **139**, No. 9, 1590–1603.

Wang, Y. H. & Tsui, K. Y. (2009). Experimental characterization of dynamic property changes in aged sands. *J. Geotech. Geoenviron. Engng* **135**, No. 2, 259–270.

Wu, J. & Helwany, S. (1996). A performance test for assessment of long-term creep behavior of soil-geosynthetic composites. *Geosynth. Int.* **3**, No. 1, 107–124.

Youn, J. U., Choo, Y. W. & Kim, D. S. (2008). Measurement of small-strain shear modulus G_{max} of dry and saturated sands by bender element, resonant column, and torsional shear tests. *Can. Geotech. J.* **45**, No. 10, 1426–1438.

Zornberg, J. G., Cabral, A. R. & Viratjandr, C. (2004). Behaviour of tire shred sand mixtures. *Can. Geotech. J.* **41**, No. 2, 227–241.